PERGAMON

International Journal of Solids and Structures 37 (2000) 5219–5231

INTERNATIONAL JOURNAL OF SOLIDS and STRUCTURES

www.elsevier.com/locate/ijsolstr

Electroelastic fracture dynamics for multilayered piezoelectric materials under dynamic anti-plane shearing

B.L. Wang*, J.C. Han, S.Y. Du

Center for Composite Materials, Harbin Institute of Technology, Harbin, 150001, People's Republic of China

Received 15 January 1998; in revised form 15 May 1999

Abstract

This paper describes a method to analyze the dynamic response of a multilayered piezoelectric material plate containing some non-collinear cracks. It is assumed that the multilayers is composed of numerous laminae with cracks located at the interface of composite layers. Based upon Fourier transforms and Laplace transforms, the boundary value problem is reduced to a system of generalized singularity integral equations in the Laplace transform domain. By utilized numerical Laplace inversion, the time-dependent full field solutions are obtained in the time domain. Numerical results are plotted to illustrate how the loading state and material non-homogeneity influence the stress fields and the electric displacement fields ahead of the crack tip.

Keywords: Multi layers; Piezoelectric materials crack; Interface; Dynamic fracture mechanics

1. Introduction

The development of piezoelectric composite materials offers great potential for use in advanced structural applications. By taking advantage of the direct and converse piezoelectric effects, piezoelectric composite structures can combine the traditional performance advantages of composite laminates along with the inherent capability of piezoelectric materials to adapt to their current environment. As piezoelectric materials are extensively used as actuators, sensors, sonar projector and medical ultrasonic imaging applications, demand for advanced piezoelectric materials with high strength, high toughness, low thermal expansion coefficient, and low dielectric constant is increasing. In an effect to obtain a piezoelectric material with these competing properties, considerable research has been directed toward

* Corresponding author. Fax: +86-451-622-1048.
E-mail address: wangbl@public.hr.hl.cn (B.L. Wang).

0020-7683/00/$ - see front matter
PII: S0020-7683(99)00218-8

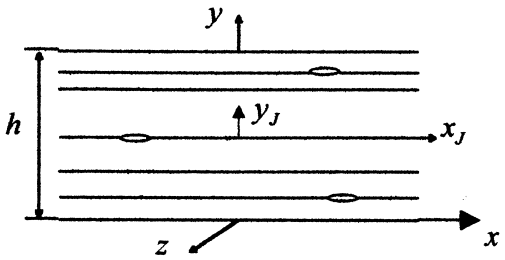

Fig. 1. Geometry and coordinates of multilayer piezoelectric medium.

the development of functionally graded or multilayered structure. However, a potential problem of multilayered materials is that delamination (i.e., cracks growth between the layers) can occur during processing.

Efforts have been made to establish electro-mechanical modeling of cracks in piezoelectric materials. Suo et al. studied cracks either in piezoelectrics, or on interfaces between piezoelectrics and other materials such as metal electrodes or polymer materials (Suo et al., 1992). They obtained closed form solutions for infinite piezoelectric medium containing a center crack. A new type of singularity is discovered around interface crack tip. Four modes of square root singularities are identified at the tip of a crack in a homogeneous piezoelectric. Shindo and his colleagues studied the static anti-plane fracture of a cracked piezoelectric strip (Shindo et al., 1990, 1996a, 1997). The dynamic representation formulas and fundamental solutions for piezoelectricity were proposed (Khutoryansky and Sosa, 1995). Shindo and his colleagues studied the dynamic response of a cracked dielectric medium under the action of harmonic waves in a uniform electric field (Shindo et al., 1996b). In the above-mentioned works, the piezoelectric media are homogeneous. We have systematically studied the multiple crack problem in non-homogeneous materials subjected to dynamic anti-plane mechanical loading (Wang et al., 1998a) and dynamic in-plane mechanical loading (Wang et al., 1998b, 1999). In present work, we expand their work to an electroelastic multiple crack problem for multilayered piezoelectric materials under longitudinal shear. Laplace and Fourier transforms techniques are used to reduce the problem to the solution of singular integral equations. Numerical calculations are carried out and the stress and electric displacement intensity factors are shown graphically for some piezoelectric ceramics.

2. Solution of the problem

Fig. 1 illustrates the geometry of an N-layers multilayer of height h with properties that vary as a function of coordinate y. (x, y, z) is the global coordinate system. y_J is the local coordinate of the Jth layer. Throughout the paper, the subscript J is associated with the Jth layer, counted up from the lower surface. The subscript j stands for the interface number between the Jth layer and the $(J + 1)$th layer. Material properties are taken to be constants for each layer. The main axis of elasticity is parallel to x- and y-axis. For the Jth layer, the density is ρ_J, thickness is h_J.

Under out-of-plane displacement $w_J(x, y_J)$ and in-plane electric potential $\phi_J(x, y_J)$, the piezoelectric boundary value problem has the form

$$(\sigma_{xz})_J = (C_{44})_J \partial w_J/\partial x + (e_{15})_J \partial \phi_J/\partial x \tag{1}$$

$$(\sigma_{yz})_J = (C_{44})_J \partial w_J/\partial y_J + (e_{15})_J \partial \phi_J/\partial y_J \tag{2}$$

$$D_x = (e_{15})_J \partial w_J/\partial x - (\epsilon_{11})_J \partial \phi_J/\partial x \tag{3}$$

$$D_y = (e_{15})_J \partial w_J/\partial y_J - (\epsilon_{11})_J \partial \phi_J/\partial y_J \tag{4}$$

The governing equations may be written in the form

$$(c_{44})_J\left(\frac{\partial^2 w_J}{\partial x^2} + \frac{\partial^2 w_J}{\partial y_J^2}\right) + (e_{15})_J\left(\frac{\partial^2 \phi_J}{\partial x^2} + \frac{\partial^2 \phi_J}{\partial y_J^2}\right) = \rho_J \frac{\partial^2 w_J}{\partial t^2}, \tag{5}$$

$$(e_{15})_J\left(\frac{\partial^2 w_J}{\partial x^2} + \frac{\partial^2 w_J}{\partial y_J^2}\right) - (\epsilon_{11})_J\left(\frac{\partial^2 \phi_J}{\partial x^2} + \frac{\partial^2 \phi_J}{\partial y_J^2}\right) = 0 \tag{6}$$

Denote the interlaminar stress $(\tau_{yz})_j$ as $\tau_j(x)$ and the interlaminar electric displacement $(D_y)_j$ as $D_j(x)$. Adjacent two layers are either perfectly bonded or are partly separated by a crack. The crack length is $2a_j$, the crack center is located in the position of $x_j = c_j$. In the problem considered, it will be assumed that the initial displacement, electric potential and velocity are zeros, and the boundary conditions have the following form:

$$\tau_j(x) = \tau_{0j}(x) \qquad D_j(x) = D_{0j}(x) \qquad c_j - a_j < x < c_j + a_j \tag{7}$$

for crack faces,

$$\tau_{yz}(x, y = 0) = \tau_0(x) \qquad D_y(x, y = 0) = D_0(x) \tag{8}$$

for lower surface of the piezoelectric medium and

$$\tau_{yz}(x, y = h) = \tau_N(x) \qquad D_y(x, y = h) = D_N(x) \tag{9}$$

for upper surface of the piezoelectric medium.

Referring to non-dimensional variable, $\bar{x} = x/h$, $\bar{y}_J = y_J/h$, $\bar{h}_J = h_J/h$, $\bar{a}_j = a_j/h$, $\bar{c}_j = c_j/h$, $(\bar{C}_{44})_J = (C_{44} + e_{15}^2/\epsilon_{11})_J$ and the shear wave velocity $(C_y)_J = \sqrt{(\bar{C}_{44})J_J/\rho_J}$. Applying Laplace transform over the time variable t and Fourier transform to the space variable x, Eqs. (5) and (6) may be solved to give the displacement and electric potential in each layer of the material:

$$w_J^*(\bar{x}, \bar{y}_J, p) = \frac{h}{2\pi}\int_{-\infty}^{+\infty}\left(e^{-|s|\lambda_J \bar{y}_J} A_{1J}(s) + e^{|s|\lambda_J \bar{y}_J} B_{1J}(s)\right)e^{-is\bar{x}}\,\mathrm{d}s \tag{10}$$

$$\phi_J^*(\bar{x}, \bar{y}_J, p) = (e_{15}/\epsilon_{11})_J w_J^*(\bar{x}, \bar{y}_J, p) + \varphi_J(\bar{x}, \bar{y}_J, p) \tag{11}$$

$$\varphi_J^*(\bar{x}, \bar{y}_J, p) = \frac{h}{2\pi}\int_{-\infty}^{+\infty}\left(e^{-|s|\bar{y}_J} A_{2J}(s) + e^{|s|\bar{y}_J} B_{2J}(s)\right)e^{-is\bar{x}}\,\mathrm{d}s \tag{12}$$

Where the quantities with superscript $*$ denote the Laplace transform, "p" is the Laplace transform parameter, $A_{mJ}(s, p)$ and $B_{mJ}(s, p)$ are unknowns to be determined $(m = 1, 2)$ $i = \sqrt{-1}$, and

$$\lambda_J = \sqrt{1 + \left[ph/\left(sC_y\right)_J\right]^2} \tag{13}$$

Substituting (10)–(12) into (2) and (4), we have the stress and the electric displacement (τ_j^*, D_j^*) at $(\bar{y}_J = \bar{h}_J)$ and $(\tau_{j-1}^*, D_{j-1}^*)$ at $(\bar{y}_J = 0)$:

$$\begin{Bmatrix} \tau_j^*(\bar{x}, p) \\ \tau_{j-1}(\bar{x}, p) \\ D_j^*(\bar{x}, p) \\ D_{j-1}(\bar{x}, p) \end{Bmatrix} = \frac{1}{2\pi} \int_{-\infty}^{+\infty} |s| \left[K_J(s)\right] \begin{Bmatrix} A_{1J}(s, p) \\ B_{1J}(s, p) \\ A_{2J}(s, p) \\ B_{2J}(s, p) \end{Bmatrix} e^{-is\bar{x}}\, \mathrm{d}s \tag{14}$$

where

$$\left[K_J(s)\right] = \begin{bmatrix} -\left(\bar{C}_{44}\right)_J \lambda_J e^{-|s|\lambda_J \bar{h}_J} & \left(\bar{C}_{44}\right)_J \lambda_J e^{|s|\lambda_J \bar{h}_J} & -(e_{15})_J e^{-|s|\bar{h}_J} & (e_{15})_J e^{|s|\bar{h}_J} \\ -\left(\bar{C}_{44}\right)_J \lambda_J & \left(\bar{C}_{44}\right)_J \lambda_J & -(e_{15})_J & (e_{15})_J \\ 0 & 0 & (\epsilon_{11})_J e^{-|s|\bar{h}_J} & -(\epsilon_{11})_J e^{|s|\bar{h}_J} \\ 0 & 0 & (\epsilon_{11})_J & -(\epsilon_{11})_J \end{bmatrix} \tag{15}$$

Applying Fourier transforms to (14) yields A_{1J}, B_{1J}, A_{2J}, B_{2J} in terms of τ_j^*, D_j^*, τ_{j-1}^*, D_{j-1}^*. The solution for each layer can thus be determined in terms of τ_j^*, D_j^*, τ_{j-1}^*, D_{j-1}^* by substituting A_{1J}, B_{1J}, A_{2J}, B_{2J} back into (10) and (12). Upon doing so, Eqs. (10) and (12) become

$$\begin{Bmatrix} w_J^*\left(\bar{x}, \bar{y}_J\right) \\ \varphi_J^*\left(\bar{x}, \bar{y}_J\right) \end{Bmatrix} = \frac{h}{2\pi} \int_{-\infty}^{+\infty} \frac{1}{|s|} \left[H_J(s, p)\right]^{\mathrm{T}} \left(\int_{-\infty}^{+\infty} \begin{Bmatrix} \tau_j(\bar{r}) \\ D_j(\bar{r}) \\ \tau_{j-1}(\bar{r}) \\ D_{j-1}(\bar{r}) \end{Bmatrix} e^{is\bar{r}}\, \mathrm{d}\bar{r} \right) e^{-is\bar{x}}\, \mathrm{d}s \tag{16}$$

in which

$$\left[H_J(s, p)\right] = \begin{bmatrix} \dfrac{\cosh\left(|s|\lambda_J \bar{y}_J\right)}{\left(\bar{C}_{44}\right)_J \lambda_J \sinh\left(|s|\lambda_J \bar{h}_J\right)} & 0 \\ \left(\dfrac{e_{15}}{\epsilon_{11}}\right)_J \dfrac{\cosh\left(|s|\lambda_J \bar{y}_J\right)}{\left(\bar{C}_{44}\right)_J \lambda_J \sinh\left(|s|\lambda_J \bar{h}_J\right)} & -\dfrac{\cosh\left(|s|\bar{y}_J\right)}{(\epsilon_{11})_J \sinh\left(|s|\bar{h}_J\right)} \\ -\dfrac{\cosh\left(|s|\lambda_J\left(\bar{y}_J - \bar{h}_J\right)\right)}{\left(\bar{C}_{44}\right)_J \lambda_J \sinh\left(|s|\lambda_J \bar{h}_J\right)} & 0 \\ -\left(\dfrac{e_{15}}{\epsilon_{11}}\right)_J \dfrac{\cosh\left(|s|\lambda_J\left(\bar{y}_J - \bar{h}_J\right)\right)}{\left(\bar{C}_{44}\right)_J \lambda_J \sinh\left(|s|\lambda_J \bar{h}_J\right)} & \dfrac{\cosh\left(|s|\left(\bar{y}_J - \bar{h}_J\right)\right)}{(\epsilon_{11})_J \sinh\left(|s|\bar{h}_J\right)} \end{bmatrix} \tag{17}$$

The interface conditions imply that both displacements and electric potentials are continuous across the bounded interface between two adjacent layers, i.e.

$$\partial w_{J+1}^*\left(\bar{x}, \bar{y}_{J+1} = 0\right)/\partial \bar{x} = \partial w_J^*\left(\bar{x}, \bar{y}_J = \bar{h}_J\right)/\partial \bar{x} \quad \text{out of crack} \tag{18}$$

$$\partial \varphi_{J+1}^*\left(\bar{x}, \bar{y}_{J+1} = 0\right)/\partial \bar{x} = \partial \varphi_J^*\left(\bar{x}, \bar{y}_J = \bar{h}_J\right)/\partial \bar{x} \text{ out of crack} \tag{19}$$

Applying Eqs. (16)–(18) and (19) show that

$$\frac{i}{2\pi}\int_{-\infty}^{+\infty}\operatorname{sgn}(s)\Big(\big[L(s)\big]_j \quad \big[M(s)\big]_j \quad \big[N(s)\big]_j\Big)e^{-is\bar{x}}$$

$$\int_{-\infty}^{+\infty}\Big\{\tau_{j-1}^*(\bar{r}) \quad D_{j-1}^*(\bar{r}) \quad \tau_j^*(\bar{r}) \quad D_j^*(\bar{r}) \quad \tau_{j+1}^*(\bar{r}) \quad D_{j+1}^*(\bar{r})\Big\}^{\mathrm{T}} e^{is\bar{r}}\,\mathrm{d}\bar{r}\mathrm{d}s = 0 \tag{20}$$

The matrices defined in these equations are

$$\big[L(s,p)\big]_j = \frac{-\begin{bmatrix}1 & e_{15}/\epsilon_{11}\\ 0 & 0\end{bmatrix}_J}{\sinh\big(|s|\lambda_J\bar{h}_J\big)\big(c_{44}+e_{15}^2/\epsilon_{11}\big)_J\lambda_J} + \frac{\begin{bmatrix}0 & 0\\ 0 & 1\end{bmatrix}}{\sinh\big(|s|\bar{h}_J\big)(\epsilon_{11})_J} \tag{21}$$

$$\begin{aligned}\big[M(s,p)\big]_j = {} & \frac{\begin{bmatrix}1 & e_{15}/\epsilon_{11}\\ 0 & 0\end{bmatrix}_J}{\tanh\big(|s|\lambda_J\bar{h}_J\big)\big(c_{44}+e_{15}^2/\epsilon_{11}\big)_J\lambda_J} - \frac{\begin{bmatrix}0 & 0\\ 0 & 1\end{bmatrix}}{\tanh\big(|s|\bar{h}_J\big)(\epsilon_{11})_J}\\ & + \frac{\begin{bmatrix}1 & e_{15}/\epsilon_{11}\\ 0 & 0\end{bmatrix}_{J+1}}{\tanh\big(|s|\lambda_{J+1}\bar{h}_{J+1}\big)\big(c_{44}+e_{15}^2/\epsilon_{11}\big)_{J+1}\lambda_{J+1}} - \frac{\begin{bmatrix}0 & 0\\ 0 & 1\end{bmatrix}}{\tanh\big(|s|\bar{h}_{J+1}\big)(\epsilon_{11})_{J+1}}\end{aligned} \tag{22}$$

$$\big[N(s,p)\big]_j = \big[L(s,p)\big]_{j+1} \tag{23}$$

Eq. (20) may be satisfied by defining new auxiliary functions $\psi_{wj}(\bar{x})$ and $\psi_{\phi j}(\bar{x})$ such that

$$\begin{aligned}&\frac{\operatorname{sgn}(s)}{i}\int_{\bar{c}_j-\bar{a}_j}^{\bar{c}_j+\bar{a}_j}\begin{Bmatrix}\psi_{wj}(\bar{x})\\ \psi_{\varphi j}(\bar{x})\end{Bmatrix}e^{is\bar{x}}\,\mathrm{d}\bar{r}\\ &\quad=\int_{-\infty}^{+\infty}\left(\big[L(s)\big]_j\begin{Bmatrix}\tau_{j-1}^*(\bar{x})\\ D_{j-1}^*(\bar{x})\end{Bmatrix}+\big[M(s)\big]_j\begin{Bmatrix}\tau_j^*(\bar{x})\\ D_j^*(\bar{x})\end{Bmatrix}+\big[N(s)\big]_j\begin{Bmatrix}\tau_{j-1}^*(\bar{x})\\ D_{j-1}^*(\bar{x})\end{Bmatrix}\right)e^{is\bar{x}}\,\mathrm{d}\bar{x}\end{aligned} \tag{24}$$

Using the mechanical traction and electric charge conditions for upper surface and lower surface of the medium, Eq. (24) can be written in matrix form

$$\big[S(s,p)\big]\int_{-\infty}^{+\infty}\big\{\Sigma(\bar{x})\big\}e^{is\bar{x}}\,\mathrm{d}\bar{x} = \frac{\operatorname{sgn}(s)}{i}\big\{\Phi(s)\big\} - \big\{\Phi_b(s)\big\} \tag{25}$$

with $\{\Phi(s)\}$ and $\{\Sigma(\bar{x})\}$ two vectors of $2(N-1)$ rows each

$$\begin{aligned}&\big\{\Phi(s)\big\} =\\ &\left\{\int_{\bar{c}_1-\bar{a}_1}^{\bar{c}_1+\bar{a}_1}\psi_{w1}e^{is\bar{r}}\,\mathrm{d}\bar{r} \quad \int_{\bar{c}_1-\bar{a}_1}^{\bar{c}_1+\bar{a}_1}\psi_{\varphi 1}e^{is\bar{r}}\,\mathrm{d}\bar{r} \quad \cdots \quad \int_{\bar{c}_{N-1}-\bar{a}_{N-1}}^{\bar{c}_{N-1}+\bar{a}_{N-1}}\psi_{w(N-1)}e^{is\bar{r}}\,\mathrm{d}\bar{r} \quad \int_{\bar{c}_{N-1}-\bar{a}_{N-1}}^{\bar{c}_{N-1}+\bar{a}_{N-1}}\psi_{\varphi(N-1)}e^{is\bar{r}}\,\mathrm{d}\bar{r}\right\}^{\mathrm{T}}\end{aligned} \tag{26}$$

$$\{\Sigma(\bar{x})\} = \{\tau_1^*(\bar{x}) \quad D_1^*(\bar{x}) \quad \cdots \quad \tau_{N-1}^*(\bar{x}) \quad D_{N-1}^*(\bar{x})\}^{\mathrm{T}} \tag{27}$$

In Eq. (25), $\{\Phi_b(s)\}$ is a vector of $2(N-1)$ rows. Only the first two elements and the last two elements in $\{\Phi_b(s)\}$ are non-zero, they are related to the boundary condition by

$$\{\Phi_{b1}(s)\} = [L_1(s)] \int_{-\infty}^{+\infty} \begin{Bmatrix} \tau_0^*(\bar{r}) \\ D_0^*(\bar{r}) \end{Bmatrix} e^{is\bar{r}}\, \mathrm{d}\bar{r} \tag{28}$$

$$\{\Phi_{b(N-1)}(s)\} = [N_{(N-1)}(s)] \int_{-\infty}^{+\infty} \begin{Bmatrix} \tau_N^*(\bar{r}) \\ D_N^*(\bar{r}) \end{Bmatrix} e^{is\bar{r}}\, \mathrm{d}\bar{r} \tag{29}$$

and

$$[S(s,p)] = \begin{bmatrix} M_1 & N_1 & & & & \\ L_2 & M_2 & N_2 & & & \\ & & \ddots & \ddots & & \\ & & & \ddots & & \\ & & & L_{N-2} & M_{N-2} & N_{N-2} \\ & & & & L_{N-1} & M_{N-1} \end{bmatrix} \tag{30}$$

Eq. (25) is the relationship between interfacial shearing stresses/electric displacements and interfacial auxiliary functions, and there are $2(N-1)$ equations in Eq. (25). For those interfaces with no crack, the auxiliary function is zero, so the number of equations needed to be solved is twice the crack number.

Let the inverse of matrix $[S(s)]$ be $[T(s)]$. Referring to variable $T_m^n(s)$, which denote the mth row and the nth column of matrix $[T(s,p)]$. Applying inverse Fourier transform to (25) yields

$$\begin{Bmatrix} \tau_j^*(\bar{x}) \\ D_j^*(\bar{x}) \end{Bmatrix} + \begin{Bmatrix} \tau_{bj}^*(\bar{x}) \\ D_{bj}^*(\bar{x}) \end{Bmatrix} = \frac{1}{2\pi i} \sum_{k=1}^{N-1} \int_{\bar{c}_k - \bar{a}_k}^{\bar{c}_k + \bar{a}_k} \left(\int_{-\infty}^{+\infty} \mathrm{sgn}(s) \begin{bmatrix} T_{(2j-1)}^{(2k-1)}(s) & T_{(2j-1)}^{(2k)}(s) \\ T_{(2j)}^{(2k-1)}(s) & T_{(2j)}^{(2k)}(s) \end{bmatrix} e^{is(\bar{r}-\bar{x})}\, \mathrm{d}s \right) \begin{Bmatrix} \psi_{wk}(\bar{r}) \\ \psi_{\phi k}(\bar{r}) \end{Bmatrix} \mathrm{d}\bar{r} \tag{31}$$

where

$$\begin{Bmatrix} \tau_{bj}^*(\bar{x}) \\ D_{bj}^*(\bar{x}) \end{Bmatrix} = \frac{1}{2\pi} \int_{-\infty}^{+\infty} \mathrm{sgn}(s) \begin{bmatrix} T_{(2j-1)}^{1}(s) & T_{(2j-1)}^{2}(s) & T_{(2j-1)}^{(2N-3)}(s) & T_{(2j-1)}^{(2N-2)}(s) \\ 0 & T_{(2j)}^{2}(s) & 0 & T_{(2j)}^{(2N-2)}(s) \end{bmatrix} \begin{Bmatrix} \Phi_{b1}(s) \\ \Phi_{b(N-1)}(s) \end{Bmatrix} e^{-is\bar{x}}\, \mathrm{d}s \tag{32}$$

In order to separate a singular part of the kernel in Eq. (31), the asymptotic behavior of the elements in matrix $[T(s)]$ for $|s| \to \infty$ must be examined. One can see from Eqs. (21)–(23) and (30) that as $|s| \to \infty$, the only non-zero elements in $[T(s)]$ are

$$T_{2j-1}^{2j-1}(\infty) = (\bar{C}_{44})_j/2 = \frac{(\bar{C}_{44})_J (\bar{C}_{44})_{J+1}}{(\bar{C}_{44})_J + (\bar{C}_{44})_{J+1}} \tag{33}$$

$$T^{2j}_{2j-1}(\infty) = (\bar{e}_{15})_j/2 = \frac{(e_{15})_J(\epsilon_{11}\bar{C}_{44})_{J+1}+(e_{15})_{J+1}(\epsilon_{11}\bar{C}_{44})_J}{((\epsilon_{11})_J+(\epsilon_{11})_{J+1})((\bar{C}_{44})_J+(\bar{C}_{44})_{J+1})} \tag{34}$$

$$T^{2j}_{2j}(\infty) = -(\bar{\epsilon}_{11})_j/2 = -\frac{(\epsilon_{11})_J(\epsilon_{11})_{J+1}}{(\epsilon_{11})_J+(\epsilon_{11})_{J+1}} \tag{35}$$

By defining $\bar{T}^n_m(s) = T^n_m(s) - T^n_m(\infty)$, one can express Eq. (31) as follows

$$\begin{Bmatrix} \tau^*_j(\bar{x}) \\ D^*_j(\bar{x}) \end{Bmatrix} + \begin{Bmatrix} \tau^*_{bj}(\bar{x}) \\ D^*_{bj}(\bar{x}) \end{Bmatrix} = \frac{1}{\pi}\sum_{k=1}^{N-1}\int_{\bar{c}_k-\bar{a}_k}^{\bar{c}_k+\bar{a}_k}\left(\int_0^{+\infty}\begin{bmatrix} \bar{T}^{(2k-1)}_{(2j-1)}(s) & \bar{T}^{(2k)}_{(2j-1)}(s) \\ 0 & \bar{T}^{(2k)}_{(2j)}(s) \end{bmatrix}\sin s(\bar{r}-\bar{x})\,\mathrm{d}s\right)$$
$$\begin{Bmatrix} \psi_{wk}(\bar{r}) \\ \psi_{\varphi k}(\bar{r}) \end{Bmatrix}\mathrm{d}\bar{r} + \frac{1}{2\pi}\begin{bmatrix} (\bar{C}_{44})_j & (\bar{e}_{15})_j \\ 0 & -(\bar{\epsilon}_{11})_j \end{bmatrix}\int_{\bar{c}_j-\bar{a}_j}^{\bar{c}_j+\bar{a}_j}\frac{1}{\bar{r}-\bar{x}}\begin{Bmatrix} \psi_{wj}(\bar{r}) \\ \psi_{\varphi j}(\bar{r}) \end{Bmatrix}\mathrm{d}\bar{r}$$

As the second row of Eq. (36) does not contain any mechanical stress term, and $\bar{T}^{(2k)}_{(2j)}(s)$ is independent on p, the mechanical boundary conditions have no influence on interfacial electric displacement.

Eq. (36) is singular integral equation having simple Cauchy-type kernels as the dominant singular parts. Note that its fundamental function corresponds to the weight function of the Chebyshev polynomial of the first kind $T_m(\bar{r}_j)$. The crack-tip stress and electric field can be characterized by standard square-root singularity. According to the singular integral equation method, Eq. (36) has the solutions of the following forms

$$\psi_{wj}(\bar{a}_j\bar{r}_j+\bar{c}_j) = \psi^0_{wj}(\bar{r}_j)/\sqrt{1-\bar{r}_j^2} = \sum_{m=1}^{M} C^m_{wj}(p)T(\bar{r}_j)/\sqrt{1-\bar{r}_j^2} \tag{37}$$

$$\psi_{\varphi j}(\bar{a}_j\bar{r}_j+\bar{c}_j) = \psi^0_{\varphi j}(\bar{r}_j)/\sqrt{1-\bar{r}_j^2} = \sum_{m=1}^{M} C^m_{\varphi j}(p)T(\bar{r}_j)/\sqrt{1-\bar{r}_j^2} \tag{38}$$

Where $\bar{r}_j=(\bar{r}-\bar{c}_j)/\bar{a}_j$, $\psi^0_{wj}(\bar{r}_j)$ and $\psi^0_{\varphi j}(\bar{r}_j)$ are continuous and bounded function on the interval $\bar{r}_j\epsilon[-1, 1]$, $(C^m_{wj}(p) \quad C^m_{\psi j}(p))$ are unknowns to be determined. M is selected to be large enough for obtaining the solutions to the defined problem with a required degree of accuracy.

Once the unknown auxiliary function $\phi_{wj}(\bar{r})$ and $\phi_{\varphi j}(\bar{r})$ are solved from (36), the interlaminar stress and electric displacement are determined. Substituting the results into (16), then (10)–(12), we can obtain the anti-plane mechanical displacement, electric potential. Using Eqs. (1)–(4), we can eventually obtain the stress and electrical displacement in each layer. The intensities of dynamic stress and electric displacement around the crack tip can be calculated as

$$(K^*_\tau)_j = \left(\sqrt{2[(c_j-a_j)-x]}\right)_{x\to(c_j-a_j)^-}\tau^*_j(\bar{x}) = -\frac{1}{2}\left((\bar{C}_{44})_j\psi^0_{wj}(-1)+(\bar{e}_{15})_j\psi^0_{\varphi j}(-1)\right)\sqrt{a_j} \tag{39}$$

$$(K^*_D)_j = \left(\sqrt{2[(c_j-a_j)-x]}\right)_{x\to(c_j-a_j)^-}D^*_j(\bar{x}) = \frac{(\bar{\epsilon}_{11})_j}{2}\sqrt{a_j}\psi^0_{\varphi j}(-1) \tag{40}$$

for left-hand side crack-tip, and

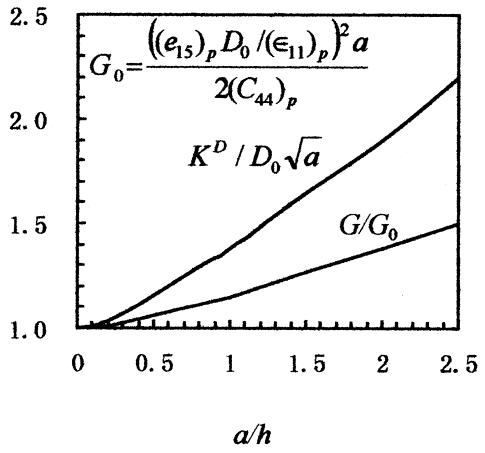

Fig. 2. Steady state electric displacement intensity factor and energy release rate versus crack length for center cracked PZT-5H ceramic under electrical load.

$$(K_\tau^*)_j=\left(\sqrt{2[x-(c_j+a_j)]}\right)_{x\to(c_j+a_j)^+}\tau_j^*(\bar{x})=\left((\bar{C}_{44})_j\psi_{wj}^0(1)+\frac{(\bar{e}_{15})_j}{2}\psi_{\varphi j}^0(1)\right)\sqrt{a_j} \tag{41}$$

$$(K_D^*)_j=\left(\sqrt{2[x-(c_j+a_j)]}\right)_{x\to(c_j+a_j)^+}D_j^*(\bar{x})=-\frac{(\bar{\epsilon}_{11})_j}{2}\sqrt{a_j}\psi_{\varphi j}^0(1) \tag{42}$$

for right-hand side crack-tip.

After the solutions in Laplace transform plane are obtained, we must use inverse Laplace transform to get the solutions in the time domain. Although there are a number of numerical methods, the one used here is due to Durbin (1974). This method works with complex data, this has important implications on the accuracy and efficiency of the method as can be seen from comparison studies given by Narayanan and Beskos (1982).

Referring to (K_S) and $(K_D)_j$ which denote the inverse Laplace transform of (K_S^*) and $(K_D^*)_j$, the energy release rates may compute by virtual crack close technique. For example, the energy release rates for right-hand side crack-tip is

$$(G(t))_j=\frac{\pi}{2}\left(\frac{1}{(\bar{C}_{44})_j}(K_S)_j^2+\frac{(\bar{e}_{15})_j}{(\bar{C}_{44})_j(\bar{\epsilon}_{11})_j}(K_S)_j(K_D)_j-\frac{1}{(\bar{\epsilon}_{11})_j}(K_D)_j^2\right) \tag{43}$$

where

$$f_{SS}=(\epsilon_{11})_J/\left[(c_{44})_J(\epsilon_{11})_J+(e_{15})_J^2\right]+(\epsilon_{11})_{J+1}/\left[(c_{44})_{J+1}(\epsilon_{11})_{J+1}+(e_{15})_{J+1}^2\right] \tag{44}$$

$$f_{SD}=(e_{15})_J/\left[(c_{44})_J(\epsilon_{11})_J+(e_{15})_J^2\right]+(e_{15})_{J+1}/\left[(c_{44})_{J+1}(\epsilon_{11})_{J+1}+(e_{15})_{J+1}^2\right] \tag{45}$$

$$f_{DD}=-(c_{44})_J/\left[(c_{44})_J(\epsilon_{11})_J+(e_{15})_J^2\right]+(c_{44})_{J+1}/\left[(c_{44})_{J+1}(\epsilon_{11})_{J+1}+(e_{15})_{J+1}^2\right] \tag{46}$$

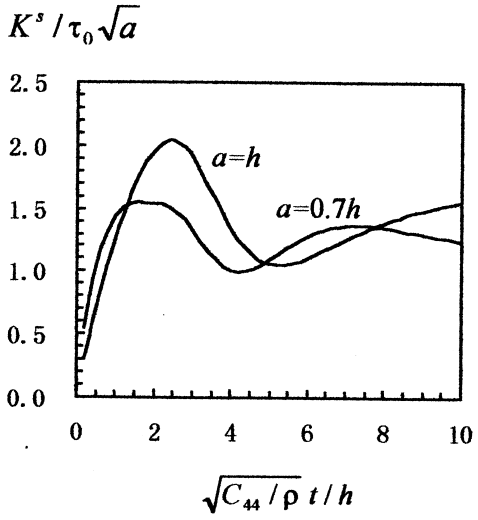

Fig. 3. Variation of stress intensity factor with time for center cracked PZT-5H ceramic under transient mechanical load.

3. Applications

In this section, we investigate the responses of some cracked piezoelectric medium. The first problem under consideration is a PZT-5H ceramic of height h with a center crack of length $2a = h$. The shear module c_{44}, the piezoelectric constant e_{15} and the dielectric constant ϵ_{11} for PZT-5H ceramic are 3.53×10^{10} N/m^2, 17 C/m^2 and 151×10^{-10} C/Vm, respectively. The mass density is denoted by ρ. To show the validity of the present method, the effect of crack length on steady electrical displacement intensity

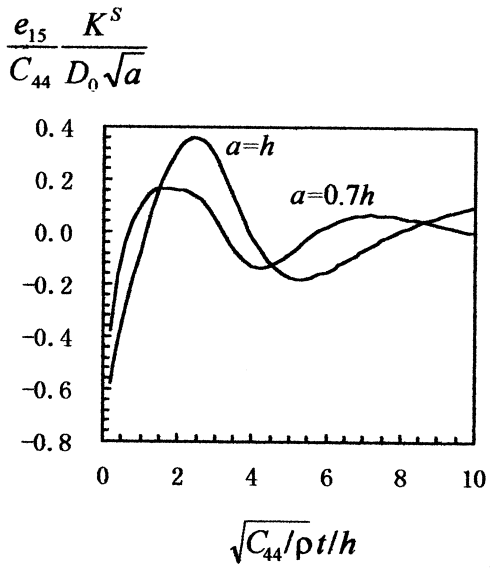

Fig. 4. Variation of stress intensity factor with time for center cracked PZT-5H ceramic under electrical load.

Table 1
The convergence of results with respect to $M(a = h)$

	$M = 5$	$M = 9$	$M = 13$	$M = 17$	$M \geq 21$
$K^{\mathrm{D}}/D_0\sqrt{a}$	1.849	1.431	1.390	1.379	1.377
$\frac{e_{15}}{C_{44}}\frac{K^{\mathrm{s}}_{\max}}{D_0\sqrt{a}}$	0.588	0.403	0.364	0.362	0.361

factors and energy release rate is plotted in Fig. 2. The results are same as that given by Shindo et al. (Shindo et al., 1997).

Assume a sudden mechanical loading τ_0 applied on crack faces. It is found that the electric displacement intensity factor is zero at the crack tip. Fig. 3 shows the variation of stress intensity factor K^{s} with time. The results are same as that for homogeneous material without piezoelectric effect. The fact demonstrates that for homogeneous materials under mechanical loading, the piezoelectric effect has no effects on stress intensity factor.

Assume a transient electric loading D_0 applied on the crack faces. It is found that the dynamic stress intensity factors are not zero and they are plotted in Fig. 4. When time t approaches to infinite, the steady stress intensity factors become zero. These results show that the stress and electric displacements are coupled in the crack plane ahead of crack tip for transient electrical load.

In numerical procedure, we have truncated the infinite series in Eqs. (37) and (38) to M terms. To validate the numerical procedure, we study the convergence of results with respect to M. Consider a transient electric loading D_0 applied on the crack faces. In this case, the electric displacement intensity factor does not vary with time and the steady state stress intensity factor is zero. The electric displacement intensity factor K^{D} and the peak stress intensity factor $K^{\mathrm{s}}_{\max}$ are tabulated in Table 1. It is clear that as M increases, the result converges to some steady values.

The approach outlined in the foregoing section is employed to investigate the response of a smart multilayered piezoelectric composite plate with two cracks. The specimen geometry and cracks positions are shown in Fig. 5. The interlayer material is graphite/epoxy composite of height $h/2$. The outer layer materials are PZT-G1195N piezoelectric ceramics of height $h/4$. The shear module, piezoelectric constant and the dielectric constant for PZT-G1195N are $(C_{44})_p = 2.42 \times 10^{10}$ N/m^2, $(e_{15})_p = 6.5$ C/m^2 and $(\epsilon_{11})_p = 153 \times 10^{-10}$ C/Vm, respectively. For graphite/epoxy, there is no piezoelectric effect, the shear module are $(C_{44})_g = 0.71 \times 10^{10}$ N/m^2. The mass density for two materials are 7600 and 1600 kg/m^3, respectively.

As mentioned in the foregoing sections, the mechanical boundary conditions have no influence on interfacial electric displacement. Assume a sudden uniform τ_0 is applied on crack faces. The results show that the electric displacement intensity factors are zero at any time t. Figs. 6 and 7 show the variation of

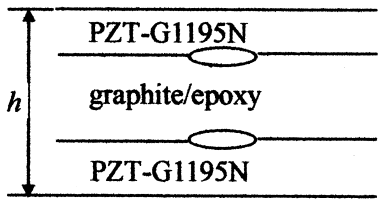

Fig. 5. Model of piezoelectric plate with attached graphite/epoxy patches.

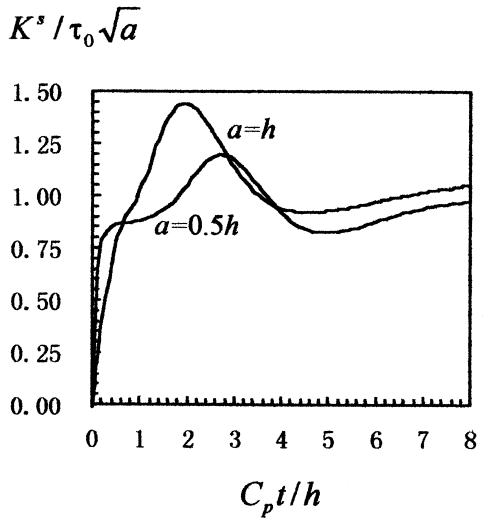

Fig. 6. Variation of stress intensity factor with time for multilayers piezoelectrics under transient mechanical load.

stress intensity factors (SIF) and energy release rate with time t (in which, C_p and $(C_{44})_p$ are respectively, the shearing wave velocity and the shear module of PZT-G1195N material).

When the piezoelectrics is sudden loaded electrically, the electric displacement intensity factor does not vary with time, while the stress intensity factors are not zero (even for steady state case when t approaches infinite) as shown in Fig. 8. This means that the inertia effect has no influence on electric displacement ahead of the crack tip under electrical loading, the stress and electric displacements are coupled in the crack plane ahead of the crack tip for non-homogeneous piezoelectric medium.

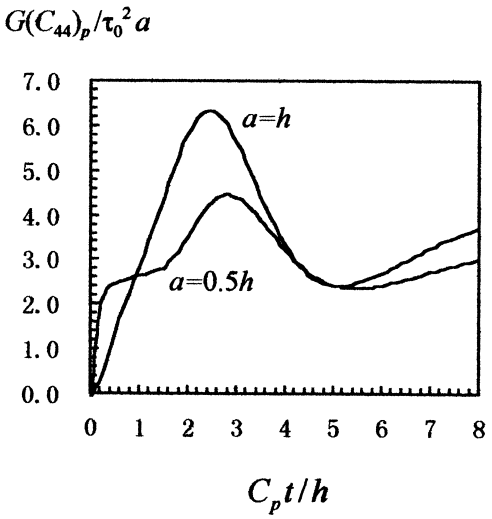

Fig. 7. Variation of energy release rate with time for multilayers piezoelectrics under transient mechanical load.

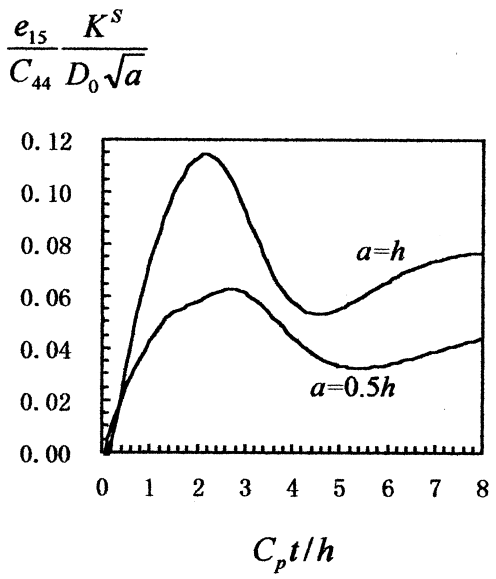

Fig. 8. Variation of stress intensity factor with time for multilayered piezoelectrics under electrical load.

4. Summary

Multilayered medium is very attractive to engineering application. This paper analyzed the electrocmechanical response of finite cracks in multilayered piezoelectrics. The problem is to compute the transient stress intensity factors and electric displacement intensity factors. Laplace and Hankel transforms are used to reduce the mixed boundary value problems to a system of singular integral equations, which are solved numerically. From the numerical example we found that the electric–mechanical fields in the crack plane ahead of the crack tip have the following behaviors.

1. Under mechanical loading, the stress field and electric displacement field are un-coupled either for homogeneous piezoelectric medium or for inhomogeneous piezoelectric medium.
2. Under electrical loading, the transient stress field and electric displacement field are coupled either for homogeneous piezoelectric medium or for inhomogeneous piezoelectric medium.
3. Under electrical loading, the steady state stress field and electric displacement field are un-coupled for homogeneous piezoelectric medium but coupled for inhomogeneous piezoelectric medium.
4. The inertia effect has no influence on electrical displacement intensity factor.

Acknowledgements

The first author's work is supported by the Post-Doctoral Science Foundation of China. We would like to thank the anonymous reviewers for their valuable comments on the paper.

References

Durbin, F., 1974. Numerical inversion of Laplace transforms: an efficient improvement to Duber and Abate's method. Comp. J 17, 371–376.

Narayanan, G.V., Beskos, D.E., 1982. Numerical operational methods for time-dependent linear problems. Int. J. Num. Meth. Engng 18, 1829–1854.

Khutoryansky, N.M., Sosa, H., 1995. Dynamic representation formulas and fundamential solutions for piezoelectric. Int. J. Solids Structures 32, 3307–3325.

Shindo, Y., Ozawa, E., Nowacki, J.P., 1990. Singular stresses and electric fields of a cracked piezoelectric strip. Applied Electromechanics in Materials 1, 77–87.

Shindo, Y., Katsura, H., Yan, W., 1996a. Dynamic stress intensity factor of a cracked dielectric medium in a uniform electric field. Acta Mechanica 117, 1–10.

Shindo, Y., Narita, F., Tanaka, K., 1996b. Electroelastic intensification near anti-plane shear crack in orthotropic piezoelectric ceramic strip. Theoretical and Applied Fracture Mechanics 25, 65–71.

Shindo, Y., Tanaka, K., Narita, F., 1997. Singular stress and electric fields of a piezoelectric ceramic strip with a finite crack under longitudinal shear. Acta Mechanica 120, 31–45.

Suo, Z., Kuo, C.-M., Barnett, D.M., Willis, J.R., 1992. Fracture mechanics for piezoelectric ceramics. J. Mech. Phys. Solids 40, 739–765.

Wang, B.L., Du, S.Y., Han, J.C., 1998a. Dynamic fracture mechanics analysis for anti- plane cracks in non-homogeneous composite material. Acta Materiae Compositae Sinica (in Chinese) 15 (4), 119–127.

Wang, B.L., Han, J.C., Du, S.Y., 1998b. Dynamic fracture mechanics analysis for composition material with material non-homogeneous in thickness direction. Acta Mechanica Solida Sinica 11 (1), 84–93.

Wang, B.L., Han, J.C. and Du, S.Y., 1999. Crack problems for non-homogeneous composite material subjected to dynamic loading. Int. J. Solids Structures, 1999, in press.